ARTICLE

High-Resolution Threshold Photoelectron Spectroscopy by Vacuum Ultraviolet Laser Velocity-Map-Imaging Method[†]

Zhou Lu, Hong Gao, Yun-tao Xu, Lei Yang, Chow-Shing Lam, Yanice Benitez, C. Y. Ng*

Department of Chemistry, University of California, Davis CA 95616, USA

(Dated: Received on December 1, 2015; Accepted on December 15, 2015)

We have obtained the high-resolution threshold photoelectron (TPE) spectra of chlorobenzene C_6H_5Cl (X^1A_1), propargyl radical C_3H_3 (X^2B_1), and allyl radical C_3H_5 (X^2A_1) by employing the vacuum ultraviolet (VUV) laser velocity-map-imaging-TPE (VUV-VMI-TPE) method. The photoelectron energy resolution of $1-2$ cm^{-1} observed for the VUV-VMI-TPE method is comparable to that achieved in VUV laser pulsed-field ionization-photoelectron (VUV-PFI-PE) measurements. Similar to VUV-PFI-PE measurements, the energy resolutions for VUV-VMI-photoelectron (VUV-VMI-PE) and VUV-VMI-TPE measurements are found to depend on the dc electric field F in V/cm used at the photoionization region for electron extraction. The decrease of the ionization thresholds of C_6H_5Cl and C_3H_3 observed as a function of F shows that the Stark shift correction for VUV-VMI-TPE measurements is governed by the formula $-3.1\sqrt{F}$ in cm^{-1}, which is half of the classical prediction of $-6.1\sqrt{F}$ in cm^{-1}. We have also measured the VUV-VMI-PE spectra of C_6H_5Cl and C_3H_5 at VUV energies near their ionization thresholds. The cationic vibrational bands observed in the VUV-VMI-PE measurements were assigned to be the vibrational progression, $n\nu_7^+$ (n=0−3), for $C_3H_5^+$. The higher experimental sensitivity and similar energy resolutions achieved in VUV-VMI-TPE compared to VUV-PFI-PE measurements make the VUV-VMI-TPE method an excellent alternative for high-resolution VUV-PFI-PE measurements.

Key words: Photoionization, Threshold photoelectron, Velocity-map imaging, Radical

I. INTRODUCTION

Due to the space charge effect, ions cannot be prepared in high concentrations. As a result, most of the conventional methods for spectroscopic measurements of neutral species cannot be directly applied to the study of ions. Spectroscopic properties of cations, such as rotational and vibrational constants and ionization energies (IEs), can be directly measured by high-resolution photoelectron spectroscopy. Thus, progress and development made in photoionization and photoelectron spectroscopy can be considered as advancement in ion spectroscopy.

Modern high-resolution photoelectron spectroscopic techniques that are based on the detection of zero kinetic energy (ZEKE) photoelectrons have their origin in the development of threshold photoelectron (TPE) measurements. The TPE spectroscopy, also previously referred to as ZEKE spectroscopy, was initiated about a half of century ago when tunable laboratory vacuum ultraviolet (VUV) photoionization sources based on monochromatized discharge radiation became available. By tuning the VUV photon energy across a photoionization transition band, the most popular approach for TPE detection involves the measurement of ZEKE photoelectrons using a dc extraction electric field and a steradiancy analyzer, which essentially consists of a metal capillary to define a small solid angle for discriminating kinetic photoelectrons. Since ZEKE photoelectrons can be collected efficiently with a small electric field, this approach has been proven to give excellent TPE detection sensitivity. Nevertheless, the inability to discriminate against kinetic electrons traveling in the same solid angle defined by the steradiancy analyzer [1], along with the relatively low optical resolutions offered by tunable laboratory VUV discharge sources, has generally limited the TPE resolution to about 20−30 meV (full-width at half-maximum, FWHM).

When a high-resolution pulsed laser is used as the photoionization source, the employment of a delayed electric field pulse (with respect to the application of the photoionization laser) for TPE extraction is expected to be effective for dispersing kinetic photoelectrons, and thus improve the TPE resolution. This idea of using a pulsed laser photoionization source together with the delayed pulsed electric field photoelectron detection has led to the development of the pulsed field ionization (PFI)-ZEKE or PFI-photoelectron (PFI-PE) spectros-

[†]Part of the special issue for "the Chinese Chemical Society's 14th National Chemical Dynamics Symposium".

*Author to whom correspondence should be addressed. E-mail: cyng@ucdavis.edu

copic technique [2−4]. The VUV-PFI-PE scheme was later understood to originate from the detection of ZEKE photoelectrons formed by Stark electric field ionization of high-n (n>100) Rydberg states populated by pulsed VUV laser excitation. Thus, the development of the PFI-PE detection method can be considered to derive from the TPE measurement scheme. Subsequent to the discovery of the laser PFI-PE technique, Zhu and Johnson introduced a variation of the PFI detection method, namely, the mass analyzed threshold ionization (MATI) detection scheme by detecting PFI-photoions (PFI-PIs) instead of PFI-PEs formed by PFI of high-n (n>100) Rydberg states [5]. Due to the need to separate prompt background ions from MATIs or PFI-PIs, the PFI-PI measurements are more difficult to perform and the achievable energy resolution is generally lower compared to that for PFI-PE measurements. Nevertheless, the PFI-PI detection provides information about the mass identity as well as the internal energy state of the photoion formed from the neutral precursor molecule, and has shown to allow the preparation of rovibronically selected molecular ions for unimolecular and bimolecular dynamics studies [6−8]. This aspect of PFI studies is not in the scope of the present experiment.

At the present time, the laser PFI-PE and PFI-PI detection techniques [9] are recognized as state-of-the-art photoionization methods, which generally offer the highest energy resolution of 1−4 cm^{-1} (FWHM). Although the VUV-PFI-PE and VUV-PFI-PI schemes are in principle applicable to all molecular systems, the application of these VUV laser PFI methods for the study of important molecular species, such as transient reaction intermediates and radicals, remains nontrivial. Since the PFI signal is derived from PFI of high-n (n>100) Rydberg species populated by photoexcitation (PEX) and the application of the electric field pulse for PFI detection is usually delayed up to a few μs with respect to the laser excitation, these high-n (n>100) Rydberg species can undergo decay induced by stray electric fields existed at the PEX/PI region. Without a careful effort to minimize stray electric fields, the PFI-PE and PFI-PI signals can be reduced, particularly in high-resolution PFI studies. This is the major disadvantage of PFI measurements.

A highly effective method for the separation and thus suppression of kinetic electrons in TPE detection is the velocity-map imaging (VMI) photoelectron (VMI-PE) scheme, which has been demonstrated previously by using a tunable laboratory VUV discharge photoionization source [10], achieving an energy resolution limited mostly by the optical bandwidth of 3−30 meV (FWHM) of the VUV discharge sources used. In addition to the merit of velocity-focusing of photoelectrons, the VMI-TPE and VMI-PE detection schemes also allow the collection of all low energy photoelectrons because a relatively high dc extraction electric field and a large imaging microchannel plate (MCP) detector can be used in VMI-PE measurements. That is, the VMI-PE and VMI-TPE detection schemes do not suffer from the signal-decay problem as in PFI measurements, and thus result in enhanced sensitivity for VMI-PE measurements.

The nature of VMI measurements is that the velocity resolution (Δv) depends only on Δr, and remains constant across the image (*i.e.*, for all the velocities), where r is the radial distance measured in term of the center of the VMI-PE image on the imaging detector. Thus, the achievable bandwidth (ΔE) in term of photoelectron kinetic energy (E) is expected to be proportional to $\sqrt{E}$ and can be significantly narrowed by lowering E [11]. This relation suggests that the highest photoelectron resolution or the narrowest ΔE value can be achieved by detecting TPEs as the VUV laser energy is scanned across the photoelectron transition bands of interest. This detection scheme is referred to the VUV-VMI-TPE method.

Both the VMI-PE measurement of neutral photoionization [12] and the slow electron velocity-map imaging (SEVI) measurement [13, 14] of anion photodetachment take advantage of the character of $\Delta E \propto \sqrt{E}$ for VMI-PE detection to achieve higher electron energy resolution. However, in many aspects, the VMI-PE and VMI-TPE measurements are different from the SEVI measurements. Photoionization of neutral species slightly below the ionization threshold is mediated by excitation to high-n Rydberg states. Due to the continuity of oscillator strength, the ionization threshold for neutral photoionization exhibits the step-function behavior [15]. The measured photoionization thresholds for neutral species can be lowered by the applied electric field in the photoionization/photoexcitation (PI/PEX) region, making it necessary to make Stark shift corrections, which is particularly important in high resolution photoelectron measurements. Anionic species have no Rydberg states; and the threshold law for anion photodetachment is proportional to $E^{(l+1/2)}$, where l is the angular momentum of the outgoing photoelectron. That is, the yield of photodetachment can be zero at true thresholds. The threshold law can also limit the photodetachment cross section to very low values at photon energies near the threshold.

Preliminary reports on the successful implementation and application of the VUV-VMI-TPE and VUV-VMI-PE detection methods for the high resolution photoelectron study of propargyl radical (C_3H_3) have been communicated [12, 16]. In this work, we present more detailed considerations and procedures on the application of these methods using C_3H_3 and allyl (C_3H_5) radicals and their cations $C_3H_3^+$ and $C_3H_5^+$ as examples. The comparison between the VUV-VMI-TPE spectra observed here and the VUV-PFI-PE spectra [17] reported previously has illustrated the excellent performance in sensitivity and resolution of the VUV-VMI-PE and VUV-VMI-TPE methods. Because the IE of chlorobenzene (C_6H_5Cl) (IE(C_6H_5Cl)=9.072 eV) has been well-established by VUV-PFI-PE measurements

DOI:10.1063/1674-0068/29/cjcp1512247

[18, 19] and is close to the IE(C_3H_3)=8.698 eV [12, 17], we have also chosen C_6H_5Cl to demonstrate the VUV-VMI-PE and VUV-VMI-TPE methods.

II. EXPERIMENTAL CONSIDERATION

In the present experimental study, two apparatuses were used, namely, the VUV laser PFI-PE apparatus and the VUV laser VMI-PE and VMI-TPE apparatus. The experimental arrangements and procedures employed in using these apparatuses for VUV-PFI-PE detections have been described in detail; and those for VUV-VMI-PE and VUV-VMI-TPE measurements have been briefly described in Refs.[12, 16]. Thus, a more detailed description for the VUV-VMI-PE and VUV-VMI-TPE measurements is given below in the present study.

Both the PFI and VMI apparatuses employed in this work were equipped with a tunable VUV laser system, which was generated by resonance-enhanced four-wave difference-frequency mixing ($2\omega_1-\omega_2$) schemes in a pulsed Kr or Xe gas jet as the nonlinear medium, where ω_1 and ω_2 represent the respective ultraviolet (UV) and visible laser frequencies generated by a UV and a visible dye laser, respectively. The UV and visible dye lasers were pumped by a common injection seeded Nd:YAG laser (Spectra-physics, GCR-290) operated at 30 Hz. The UV ω_1 frequency was fixed at 212.556 nm (222.560 or 249.629 nm) to match the two-photon ($2\omega_1$) resonances of the Kr (Xe) transitions. The visible ω_2 output was scanned in the range of 485−760 nm to generate the desired VUV ($2\omega_1-\omega_2$) output range of 8.1−9.4 eV as required for the present experiment [16, 20, 21]. Here, the tunable VUV ($2\omega_1-\omega_2$) output was selected by an off-axis plano-convex MgF_2 lens before entering the PEX/PI region; and its intensity was monitored by a Cu photoelectric detector. The optical bandwidth of the VUV laser output was measured to be 0.12 cm^{-1} (FWHM) for the VUV-PFI-PE apparatus [20, 21] and 0.45 cm^{-1} (FWHM) for the VUV-VMI-PE and VUV-VMI-TPE apparatus [22−26].

A. The VUV-PFI-PE apparatus

As described above, the VUV-PFI-PE apparatus consists of a pulsed (30 Hz) tunable VUV laser system as the photoionization source, a pulsed supersonic beam production system to introduce the gaseous sample, a time-of-flight (TOF) mass spectrometer for photoion detection, and a photoelectron spectrometer for PFI-PE detection. The TOF ion mass spectrometer and the TOF electron spectrometer are situated above and below the PI/PEX center, such that the central axes of the TOF ion mass spectrometer and TOF electron spectrometer are perpendicular to the traveling direction of the molecular beam.

Using the VUV-PFI-PE apparatus along with procedures described previously [20, 21, 27−29], we have measured the VUV-PFI-PE spectra of C_6H_5Cl near its ionization threshold. In this experiment, the C_6H_5Cl vapor pressure at room temperature (11.8 Torr) was seeded in He to a total stagnation pressure of 30 psi prior to supersonic expansion through a pulse valve (General valve, repetition rate=30 Hz). The resulting C_6H_5Cl pulsed beam was skimmed by a conical skimmer (diameter=2 mm) before intersecting perpendicularly with the VUV ($2\omega_1-\omega_2$) laser beam in the PI/PEX center. The timings of operating the pulsed valve and the VUV photoionization laser were synchronized by delayed pulse generators (Stanford Research System, DG535).

B. The VUV-VMI-PE and VUV-VMI-TPE apparatus

The VUV-VMI-PE and VUV-VMI-TPE apparatus was modified from the VUV laser VMI-photoion (VMI-PI) apparatus, which has been described in detail [22, 23, 30]. Since electrons are susceptible to perturbation by the Earth and stray magnetic fields, we have shielded the electron-imaging lenses and the electron TOF tube of the apparatus by two layers of μ metals. The VUV-VMI-PE and VUV-VMI-TPE apparatus, in sequential order, consists of a pulsed molecular beam production system, a set of VMI aperture lenses, a 75-cm electron TOF tube, and a VMI-PE detector. The VMI-PE detector comprises of a dual set of electron-imaging MCPs (diameter=75 mm), a P47 phosphor screen, and a CCD camera.

In the present experiment, the gas sample was seeded in He or Ar to a total stagnation pressure of 30 psi prior to supersonic expansion into the beam source chamber through a pulsed valve (Evan-Lavie Model: EL-5-2004, nozzle diameter=0.2 mm, 30 Hz). The gas sample beam thus produced traveled along the central axes of the VMI lenses and the VMI-PE detector, and was skimmed by two conical skimmers (diameter=1 mm) before entering the PI/PEX region to intersect perpendicularly the VUV ($2\omega_1-\omega_2$) laser beam. The photoelectrons thus formed were velocity-focused and mapped onto the electron-imaging MCP detector [31]. When collecting photoelectron images, the front MCP plate was grounded at all time, and a dc voltage of around +1.5 kV was applied to the second MCP plate. The amplitude of this dc voltage applied can alter the amplification of the photoelectron signal. Thus, the actual amplitude was adjusted depending on the signal level. A high voltage was applied to the P47 phosphor and the resulting fluorescence was captured by a CCD camera and transferred to a computer using the DAVIS7 software provided by LaVision. The images recorded represent 3-dimensionsal (3D) Newtonian spheres mapped onto the 2D detector plane. The 3D distribution of photoelectrons can be reconstructed

DOI:10.1063/1674-0068/29/cjcp1512247

from the recorded 2D VMI-PE image by the inverse Abel transformation [32]; and thus the kinetic energy distribution of photoelectrons can be obtained from the reconstructed 3D VMI-PE images.

We have measured the VUV-VMI-PE and VUV-VMI-TPE spectra of C_6H_5Cl, C_3H_3 and C_3H_5 near their ionization thresholds. A supersonically cooled radical beam source based on 193.3 nm laser photodissociation of propargyl chloride (C_3H_3Cl) and allyl bromide (C_3H_5Br) was used to prepare the C_3H_3 and C_3H_5 radicals, respectively [12, 16, 20, 33]. The C_3H_3Cl (C_3H_5Br) precursor sample was introduced into the beam source chamber as a gas jet of ∼10% C_3H_3Cl (C_3H_5Br) seeded in He. The 193 nm ArF excimer laser pulse (GAM laser, pulse energy≈10 mJ, repetition rate=30 Hz) intersects the precursor sample jet at the tip of the nozzle, inducing the formation of C_3H_3 (C_3H_5) radicals from photodissocation of C_3H_3Cl (C_3H_5Br). It has been demonstrated previously that radicals, such as C_3H_3 and C_3H_5 formed in the high pressure region of the pulsed jet can undergo supersonic cooling by collisions with He or Ar atoms in the jet. The supersonically cooled C_3H_3 (C_3H_5) radical beam passed through two conical skimmers (diameter=1 mm) before intersecting the tunable VUV laser radiation at the PI/PEX region of the VUV-VMI apparatus.

The imaging MCP detector used has an active area with a diameter of 75 mm, and the distance between the PI/PEX center and the center of the MCP detector is 747 mm. The photoelectron signal arriving at the MCP is monitored by the 960 pixel×960 pixel area. For VMI-TPE measurements of C_3H_3, C_3H_5, and C_6H_5Cl, the smallest central image area of 0.5 mm×0.5 mm (3 pixels×3 pixels) was used to gate the VUV-VMI-TPE counts. Thus, the critical solid angle that characterizes the steradiancy TPE detector is very small, corresponding to a very high TPE energy resolution. The optimal resolution of the VMI-TPE technique can be achieved by lowering the electric field applied at the PI/PEX region and reducing the pixel area at the center of the VMI-PE image during the scan of VUV laser energy. The VUV-VMI-TPE spectra obtained by scanning the VUV energy are normalized by the VUV intensities recorded by a Cu photoelectric detector.

III. RESULTS AND DISCUSSIONS

A main motivation of the present study of C_6H_5Cl, C_3H_3, and C_3H_5 and their cations is to establish proper procedures for VUV-VMI-PE and VUV-VMI-TPE measurements as a general method for high-resolution photoelectron spectroscopic studies.

A. VUV-PFI-PE, VUV-VMI-PE, and VUV-VMI-TPE measurements for $C_6H_5Cl^+(X^2B^1)$

The study of a stable molecule such as C_6H_5Cl is aimed to illustrate the important consideration and procedures involved in the application of the VUV-VMI-PE and VUV-VMI-TPE methods. As an example, we show in Fig.1(a) the VUV-VMI-PE image for the formation of $C_6H_5Cl^+(X^2B_1)$ obtained at $h\nu$(VUV)=9.240 eV and F=33.2 V/cm. On the basis of inverse Abel transformation and the consideration of VUV photon energy, this photoelectron image was converted to the VUV-VMI-PE spectrum for $C_6H_5Cl^+(X_2B_1)$ as shown in Fig.1(b). The photoelectron bands of $C_6H_5Cl^+(X^2B_1)$ resolved in Fig.1(b) correspond to the VMI-PE rings observed in Fig.1(a).

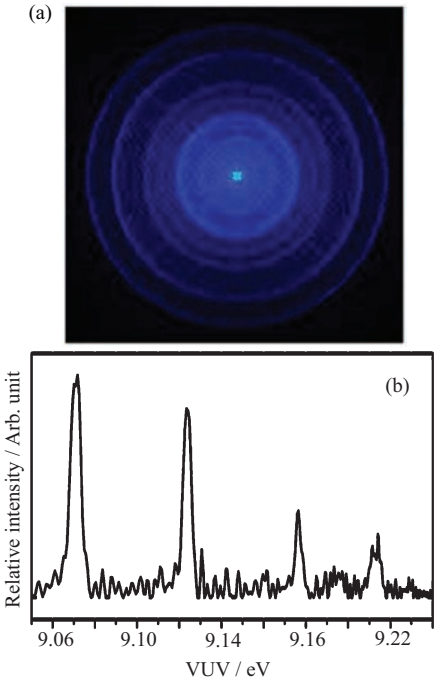

FIG. 1 (a) VUV-VMI-PE image recorded at $h\nu$ (VUV)=9.240 eV and F=33.2 V/cm. (b) VUV-VMI-PE spectrum for the formation of $C_6H_5Cl^+(X^2B_1)$ converted from the VMI-PE image shown in (a).

The VUV-VMI-PE spectrum observed at $h\nu$(VUV)=9.240 eV is compared to VUV-VMI-PE spectra for $C_6H_5Cl^+(X^2B_1)$ measured at other $h\nu$(VUV) values of 9.110, 9.150, 9.185, 9.200, 9.220, 9.290, 9.340, 9.377, 9.425, and 9.450 eV in Fig.2. The downward pointing red arrows marked the actual $h\nu$(VUV) energies used for individual VUV-VMI-PE measurements. The VMI-PE spectra reveal the excitation of two major vibrational progressions, nv_{6a} and $v_{7a}+nv_{6a}$, n=0−2, as marked on top of the spectra in Fig.2. The present measurement yields 420±5 and 1120±5 cm^{-1} for the v_{6a} and v_{7a} vibrational frequencies, respectively, which are in good agreement with the previous (1+1′) PFI-PE measurements [19].

The comparison of Fig.2 shows that as $h\nu$(VUV) is decreased, the number of vibrational bands observable in the VUV-VMI-PE spectrum is reduced because of the reduced photoelectron kinetic energy span, which is

DOI:10.1063/1674-0068/29/cjcp1512247

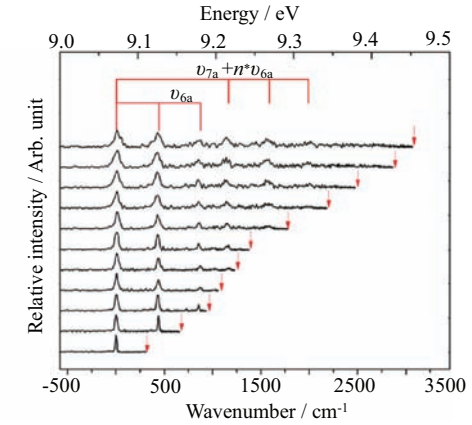

FIG. 2 The VUV-VMI-PE spectra for $C_6H_5Cl^+(X^2B_1)$ converted from VUV-VMI-PE images measured at the $h\nu$(VUV)=9.110, 9.150, 9.185, 9.200, 9.220, 9.240, 9.290, 9.340, 9.377, 9.425, and 9.450 eV and F=33.2 V/cm. The red downward pointing arrows represent the actual $h\nu$(VUV) values used for individual VUV-VMI-PE measurements. The top energy scale is the VUV energy in eV; and the bottom energy scale is in cm^{-1} measured with respect to the peak of $C_6H_5Cl^+$ origin band. The vibrational assignments are marked by red droplines on top of the figure. The excitation of two major vibrational progressions, nv_{6a} and $v_{7a}+nv_{6a}$, n=0−2, are observed as marked on top of the figure.

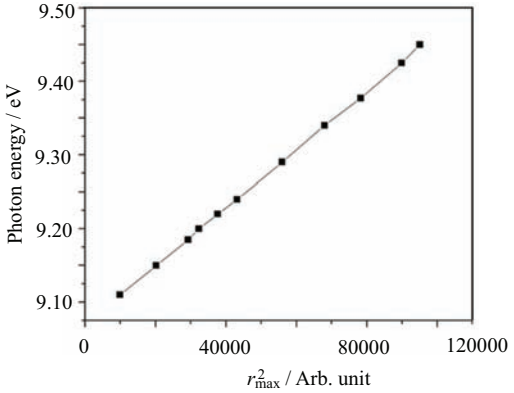

FIG. 3 The plot of $h\nu$(VUV) versus r^2_{max}, where r_{max} in arbitrary units represents the radius of the outmost ring of the VMI-PE image for the $C_6H_5Cl^+(X^2B_1)$ origin band measured at selected $h\nu$(VUV) values of 9.110, 9.150, 9.185, 9.200, 9.220, 9.240, 9.290, 9.340, 9.377, 9.425, and 9.450 eV and F=33.2 V/cm. A linear plot is observed, yielding an intercept of 9.070 eV at r_{max}=0.

determined by the difference between the $h\nu$(VUV) employed and the origin band position of $C_6H_5Cl^+(X^2B_1)$. As pointed out above concerning the application of the VMI-PE method, the kinetic energy of photoelectrons ejected from a vibrational band is proportional to the square of photoelectron velocity, and thus to r^2, where r is the radius of the VMI-PE ring observed on the imaging MCP detector. For a given $h\nu$(VUV), the outermost VMI-PE ring (radius=r_{max}) observed in this experiment correspond to the formation of the origin band of $C_6H_5Cl^+(X^2B_1)$. Thus, we expect that $h\nu$(VUV) used is proportional to r^2_{max}. This expectation is confirmed by the excellent linear plot of $h\nu$(VUV) versus r^2_{max} plot observed in Fig.3. This linear plot yields an intercept of 9.070 eV at r_{max}=0. This value can be taken as the ionization threshold of C_6H_5Cl at a dc electric field F=33 V/cm. To determine the IE(C_6H_5Cl) value from this intercept based on the VUV-VMI-PE measurements of Fig.2 requires the Stark shift correction. Since the IE(C_6H_5Cl)=73172.1±1.6 cm^{-1} has been determined by the VUV-PFI-PE measurement [18, 19], a simple energy calibration of the VUV-VMI-PE spectra would involve normalizing the peak position of the VUV-VMI-PE origin band to the latter IE(C_6H_5Cl) value.

The comparison of the VUV-VMI-PE spectra in Fig.2 also reveals that as the photoelectron kinetic energy E for a selected vibrational band is decreased due to the lowering of the $h\nu$(VUV) value, the FWHMs for the vibrational bands appearing in the spectra become narrower, indicative of higher energy resolutions at lower E values. This observation is as pointed out above. The FWHM for the origin band obtained $h\nu$(VUV)=9.110 eV is 25 cm^{-1}, and is the lowest value observed in Fig.2. Spectral simulation indicated that this FWHM value represents a limit set by overlapping rotational transitions and the rotational temperature achieved in supersonic expansion for the C_6H_5Cl molecular beam.

The relation of $\Delta E \propto \sqrt{E}$ observed in the VUV-VMI-PE measurement of C_6H_5Cl indicates that the highest resolution can be achieved by using the VUV-VMI-TPE method. This method involves scanning the $h\nu$(VUV) energy across the vibrational band of interest and gating the TPEs arriving at the center of the VMI-PE detector. We have recorded the VUV-VMI-TPE spectrum for $C_6H_5Cl^+(X^2B_1)$ in the $h\nu$(VUV) range of 9.05−9.22 eV, and this spectrum is compared in Fig.4 with the VUV-PFI-PE spectrum for $C_6H_5Cl^+(X^2B_1)$ measured in the range of 9.05−9.42 eV. The VUV-PFI-PE spectrum has been corrected for the Stark shift effect, and thus the IE(C_6H_5Cl) is marked by the peak of the VUV-PFI-PE origin band. Due to the Stark shift effect, the vibrational peaks observed in the VUV-VMI-TPE spectrum are red shifted with respect to the corresponding vibrational peak resolved in the VUV-PFI-PE spectrum. The assignment of the vibrational bands is marked on top of the spectra in the figure. In addition to the strong v_{6a} and v_{7a} vibrational bands, weak vibrational bands attributable to v_1 and v_{12} vibrational excitations are also observed in these spectra. Previous simulation of the VUV-PFI-PE origin band indicates that the PFI-PE resolution achieved was 1.5−2.0 cm^{-1} (FWHM). The essentially identical structures and FWHMs (≈25 cm^{-1}) for the vibrational

DOI:10.1063/1674-0068/29/cjcp1512247

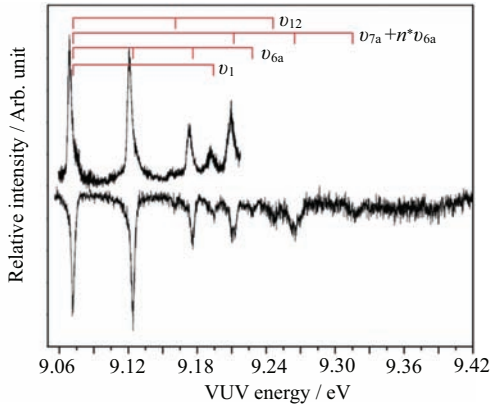

FIG. 4 (a) Comparison of the VUV-VMI-TPE spectrum (upper curve) with the VUV-PFI-PE spectrum (lower curve) for $C_6H_5Cl^+$ measured in the $h\nu$(VUV) range of 9.05−9.42 eV and F=33.2 V/cm. The VUV-VMI-PE spectrum has not been corrected for the Stark shift effect, whereas the Stark shift for the VUV-PFI-PE spectrum has been corrected by normalizing the VUV-PFI-PE origin band of $C_6H_5Cl^+$ to the IE(C_6H_5Cl). The vibrational assignments are marked by red droplines on top of the spectra.

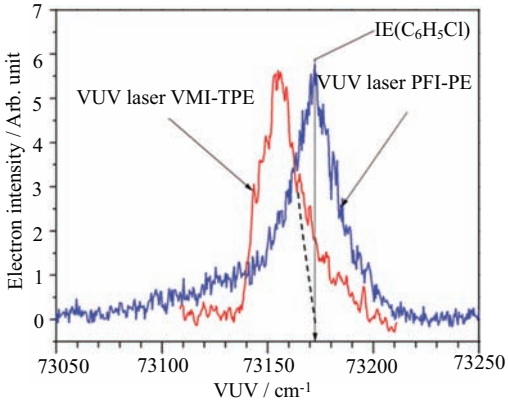

FIG. 5 A magnified plot of the VUV-VMI-TPE spectrum (red curve) and the VUV-PFI-PE spectrum (blue curve) for the origin vibrational band of $C_6H_5Cl^+$ in the energy range of 73050−73250 cm^{-1}. The VUV-PFI-PE spectrum has been corrected for the Stark shift effect. The vertical downward pointing arrow, which passes through the peak of the VUV-PFI-PE spectrum marks the IE(C_6H_5Cl). The peak position of the VUV-VMI-PE spectrum is 17 cm^{-1} lower than that of the VUV-PFI-PE spectrum, attributing to the Stark shift induced by the dc field of F=33.2 V/cm used in the VUV-VMI-PE measurement. The dashed line gives the estimated profile of the VMI-TPE spectrum. The intensities above the dashed line can be attributed as the hot photoelectron background [16].

bands observed in the VUV-VMI-TPE and the VUV-PFI-PE spectra of Fig.4 support the conclusion that the photoelectron energy resolution attained in the VUV-VMI-TPE measurement is comparable to that observed in the VUV-PFI-PE detection.

Although the FWHMs of vibrational peaks resolved in the VUV-VMI-TPE and VUV-PFI-PE spectra of Fig.4 are about the same, the energy profiles observed for the VUV-PFI-PE peaks appear to be different from those of the VUV-VMI-TPE peaks. In order to examine the different energy profile of the VUV-PFI-PE and VUV-VMI-TPE vibrational band for $C_6H_5Cl^+$, we show in Fig.5 the magnified VUV-PFI-PE and the VUV-VMI-TPE spectra for the origin band of $C_6H_5Cl^+(X^2B_1)$. The IE(C_6H_5Cl) is marked by the downward pointing blue arrow or the VUV-PFI-PE peak as the VUV-PFI-PE spectrum has been corrected for the Stark shift due to the pulsed electric field applied in the PFI-PE measurement. The different spectral characteristics observed in the VUV-VMI-TPE and VUV-PFI-PE measurements have been briefly discussed previously [16]. As shown in Fig.5, both of these spectra are asymmetric. The VUV-PFI-PE origin band for $C_6H_5Cl^+(X^2B_1)$ shows higher intensities on the low energy side of the origin band, which have been attributed to forced autoionization in VUV-PFI-PE measurements [4]. The VUV-VMI-TPE spectrum reveals higher intensities on the high energy side due to contribution from hot photoelectrons, resulting in a tailing structure toward higher energies. The discrimination of hot photoelectrons in the present detection of TPEs or ZEKE photoelectrons is achieved by the VMI-PE arrangement, such that the TPEs are expected to arrive at the center of the imaging MCP detector.

B. DC Stark shift in VMI-TPE measurements for $C_6H_5Cl^+(X^2B_1)$

A dc electric field F=33.5 V/cm was applied at the PI/PEX region in the VMI-TPE measurement of the $C_6H_5Cl^+(X^2B_1)$ origin band shown in Fig.4 and Fig.5. In an ideal situation of achieving completed discrimination of hot photoelectrons, the transmission for true TPEs is zero at the VUV energies above IE(C_6H_5Cl). Furthermore, we expect the energy profile for VMI-PE detection is a symmetric function. We have estimated the energy profile for the true VUV-VMI-TPE detection by drawing the dashed line in Fig.5 to separate the hot photoelectron contribution. That is, the signal above the dashed line are attributed to hot electrons travelling perpendicular to the MCP detector and arriving at the center of the VMI-PE image. The peak position of the $C_6H_5Cl^+$ origin band observed in the VUV-VMI-TPE spectrum is found to be 17 cm^{-1} lower than that found in the VUV-PFI-PE spectrum. This finding provides an estimate that the Stark shift correction from the true IE(C_6H_5Cl) is $-3.1\sqrt{F}$ in cm^{-1}, which is half of the value predicated by classical formula of $-6.1\sqrt{F}$ in cm^{-1}.

The PFI-PE method is based on the detection of ZEKE photoelectron originating from delayed PFI of

DOI:10.1063/1674-0068/29/cjcp1512247

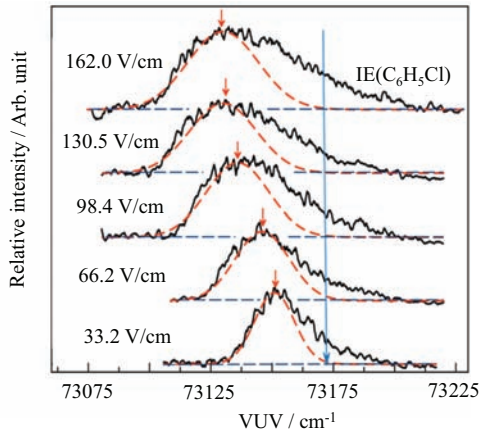

FIG. 6 The VUV-VMI-TPE spectra of the origin vibrational band of $C_6H_5Cl^+$ in the energy region of 73075−73225 cm^{-1} measured at the dc electric field F=33.2, 66.2, 98.4, 130.5, and 162.0 V/cm. The vertical blue arrow marks the IE(C_6H_5Cl). The dashed curves are the Gaussian function fits to individual VUV-VMI-TPE bands. The intensities above the dashed curves at the high energy side of the VUV-VMI-TPE peak can be attributed to contribution of hot photoelectron background.

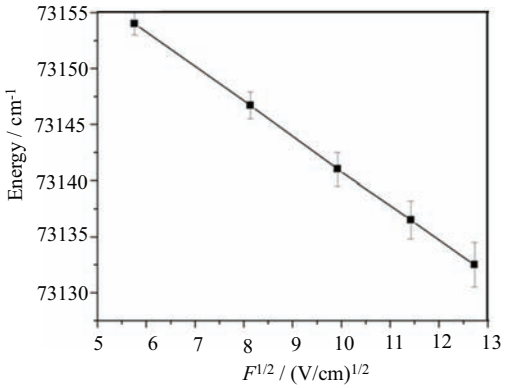

FIG. 7 Plot of the peak position of the VUV-VMI-TPE spectrum for the $C_6H_5Cl^+$ origin band versus the square root of the dc electric field F used for photoelectron extraction. The solid line represents a linear least squares fit to the plot, giving a slope of −3.10±0.01 $cm^{-1}/(V/cm^{-1})^{1/2}$ and an intercept of 73171.83±0.13 cm^{-1} at F=0.

high-n (n>100) Rydberg states by a delayed, PFI field after laser excitation. It is well-established that the lowering of the ionization threshold in delayed PFI detection is governed by the diabatic formula $-4\sqrt{F}$ in cm^{-1} [34]. To our knowledge, a detailed examination of the electric field effects on the VMI-PE and VMI-TPE methods has not been reported. We have performed a series of VUV-VMI-TPE measurements for the $C_6H_5Cl^+(X^2B_1)$ origin band at the dc electric fields of F=33.2, 66.2, 98.4, 130.5, and 162.0 V/cm. These spectra obtained without the Stark shift correction are depicted in Fig.6. The vertical line shown in the figure marks the IE(C_6H_5Cl) value determined in previous VUV-PFI-PE measurements. As shown in the figure, the increase of the dc electric field F results in shifting of the VMI-TPE origin band to a lower $h\nu$(VUV) value together with broadening of the VMI-TPE origin band. All the VMI-TPE peaks observed in Fig.6 have a similar intensity profile, *i.e.*, it drops rapidly on the low energy side and exhibits a tailing structure on the high energy side. We find that the VMI-TPE peaks observed can be simulated well by a Gaussian function except the tailing structure toward higher energies as shown by the dashed curves of Fig.6. The intensities above the dashed curves can be attributed to hot photoelectrons. While the broader VMI-PE peaks observed at a higher F field correspond to higher photoelectron intensities and thus better experimental sensitivity, the energy resolution observed is lower at a higher F value.

According to the Stark shift observed in the VUV-VMI-TPE spectrum of Fig.5, the Stark shift induced by a F field can be estimated by the formula, $-3.1\sqrt{F}$ in cm^{-1}. For the dc electric fields of F=33.2, 66.2, 98.4, 130.5, and 162.0 V/cm are predicted to be 35, 50, 61, 70, and 78 cm^{-1}, respectively. These Stark shift values were found to be consistent with the VUV-VMI-TPE peak positions observed in Fig.6. The Gaussian fits to individual VMI-PE peaks for F=33.2, 66.2, 98.4, 130.5, and 162.0 V/cm are shown as the dashed red curves in Fig.6. The center positions of the best fit Gaussian curves are also in agreement with the peak positions of the VMI-TPE spectra. The center peak positions of the $\sqrt{F}$ in Fig.7. The solid line is the linear least squares fit to the data with a slope of −3.10±0.01 $cm^{-1}(V/cm)^{-1/2}$ and an intercept of 73171.83±0.13 cm^{-1}. Since the latter value is the ionization threshold measured at F=0, it can be identified as the IE(C_6H_5Cl). Thus, this least square analysis provided a more precise IE value compared to the values determined in previous VUV-PFI-PE measurements. Furthermore, the least squares fit of Fig.7 also provides a more precise formula, $(-3.10\pm0.01)\sqrt{F}$ in cm^{-1}, for the Stark shift correction for the present VUV-VMI-TPE measurements.

C. VUV-VMI-TPE measurements of C_3H_3 and C_3H_5

The high resolution photoelectron studies of C_3H_3 and C_3H_5 radicals have been made in previous VUV-PFI-PE measurements [17, 35, 36]. Recently, we have shown that high resolution studies of transient radicals, such as C_3H_3, can also be performed using the VUV-VMI-PE and VUV-VMI-TPE methods [12, 16]. The present study provides further examinations of the dc electric field effect on the photoionization of C_3H_3 and C_3H_5 radicals.

Figure 8 depicts the VUV-VMI-TPE spectra for the origin band of $C_3H_3{}^+(X^1A_1)$ obtained at the ap-

DOI:10.1063/1674-0068/29/cjcp1512247

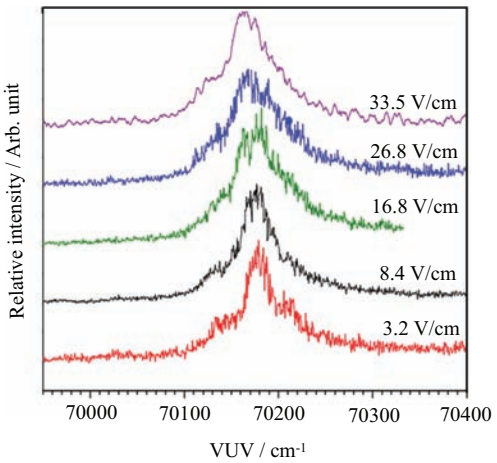

FIG. 8 The VUV-VMI-TPE spectra for the origin vibrational band of $C_3H_3^+$ measured at the dc electric fields of F=3.2, 16.8, 26.8, and 33.5 V/cm. The C_3H_3 sample was prepared by a pulsed supersonically cooled radical beam source based on 193 nm photodissociation of C_3H_3Cl. All VUV-VMI-PE spectra have been corrected for the dc Stark shift according to the formula $-3.1\sqrt{F}$ cm^{-1}.

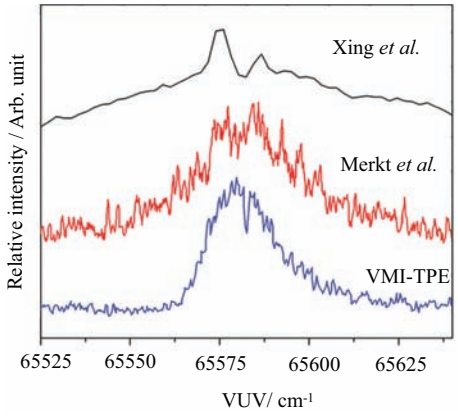

FIG. 9 Comparison of the VUV-MI-PE spectrum (bottom) for the $C_3H_5^+$ origin band with the VUV-PFI-PE spectra for the $C_3H_5^+$ origin band obtained by Xi *et al.* (top) and Gasser *et al.* [35] (middle). The VUV-VMI-TPE spectrum was obtained by setting the dc electric field F=3.2 V/cm. The VUV-VMI-TPE and the VUV-PFI-PE spectra have been corrected for the Stark shift effect.

plied dc electric fields of F=3.2, 8.4, 16.8, 26.8, and 33.5 V/cm. The comparison of these spectra reveals that the FWHM for the VUV-VMI-TPE origin band increases as F is increased. All these spectra have been corrected for the dc Stark shifts according to the formula derived above ($-3.1\sqrt{F}$ cm^{-1}). At F=33.5 V/cm, the VMI-TPE spectrum reveals a left shoulder structure on the lower energy of the main peak, while a right shoulder structure is not noticeable. As the dc electric field is decreased to 3.2 V/cm (the bottom trace in Fig.8), the right shoulder structure becomes discernible. The VUV-VMI-TPE spectrum obtained at F=3.2 V/cm is in excellent agreement with that reported recently by Gao *et al.* after taking into account the experimental uncertainties. The simulation (to be presented below) of the VUV-VMI-TPE spectrum obtained at F=3.2 V/cm yielded an IE(C_3H_3) (70174±2 cm^{-1}), which is identical to the value derived from the recent VUV-VMI-TPE measurement by Gao *et al.* [16] and that from the VUV-PFI-PE measurements by Jacovella *et al.* [17].

Figure 9 compares the VUV-PFI-PE spectra for the $C_3H_5^+(X^1A_1)$ origin band measured by Xi *et al.* [36] (top curve) and Gasser *et al.* [35] (middle curve) with that recorded by the present VUV-VMI-TPE measurement (bottom curve). All three experiments used a pulsed supersonic molecular beam source to introduce the radical sample into the PI/PEX center. The VUV-PFI-PE experiment of Xi *et al.* used a radical beam source based on pyrolysis, and thus the rotational temperature achieved was higher and thus the FWHM of the origin band is larger compared to that attained in the experiment of Grasser *et al.* and the present VUV-VMI-TPE experiment, which used a supersonic radical beam source based on 193 nm photodissociation. The dc electric field used was F=3.2 V/cm; and the VUV-VMI-TPE spectrum of Fig.9 has been corrected for the Stark shift. The double peak structure resolved in the VUV-PFI-PE spectra has been shown to arise from partially resolved rotational contours based on spectral simulations to be presented below.

D. Simulation of the origin bands for $C_3H_3^+(X^1A_1)$ and $C_3H_5^+(X^1A_1)$

The observation of partially resolved rotational contours in the VUV-VMI-TPE spectra allows rotational simulations of the VUV-VMI-TPE origin bands of $C_3H_3^+(X^1A_1)$ and $C_3H_5^+(X^1A_1)$ as shown in Fig.10 and Fig.11, respectively. Although the semi-empirical simulation presented below cannot be considered as definitive, it is useful for providing a more precise IE value and a more reliable spectral assignments. The semi-empirical simulation procedures have been discussed in detail previously, and thus only a brief description of the selection rules for the molecular symmetry group C_{2v}(M) is given below [16, 17, 35−39].

Since both the neutral and cationic C_3H_3 ($C_3H_3^+$) and C_3H_5 ($C_3H_5^+$) systems belong to the molecular symmetry group C_{2v}(M), the asymmetric top rotational energy levels can be labeled as $J''_{K_a''K_c''}(J^+_{K_a^+K_c^+})$, where $J''(J^+)$ is the total angular momentum quantum number and $K_a''(K_a^+)$ and $K_c''(K_c^+)$ are the projection quantum numbers of the neutral (cation). By using the previous reported rotational constants A″, B″, and C″ (A^+, B^+, and C^+) of C_3H_3 ($C_3H_3^+$) and C_3H_5 ($C_3H_5^+$) [16, 35, 36], the Ray's asymmetry parameters, defined as (2B″-A″-C″)/(A″-C″) for the neutral and ($2B^+$-A^+-

DOI:10.1063/1674-0068/29/cjcp1512247

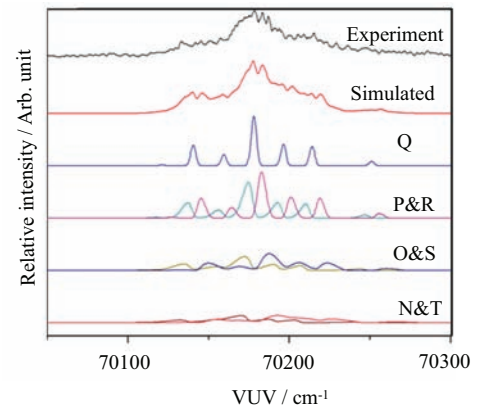

FIG. 10 Comparison of the VUV-VMI-TPE spectrum for the origin band of $C_3H_3^+$ in the region of 70050−70300 cm^{-1} with the best simulated spectrum, which is the sum of all rotational branch contributions (shown below the best simulated spectrum). The simulation is based on the selection rules that ΔK_a=odd and ΔK_c=even and odd. The simulation uses a Gaussian instrumental profile (FWHM=3.5 cm^{-1}), assumes a rotational temperature of 35 K, and the rotational branch ratios of N:O:P:Q:R:S:T=2:3:5:3:5:3:2.

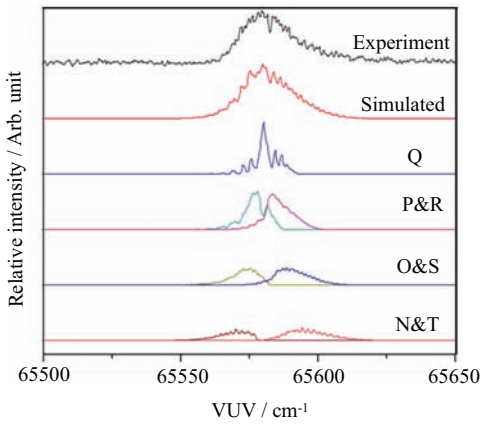

FIG. 11 Comparison of the VUV-VMI-TPE spectrum (top spectrum) for the origin band of $C_3H_5^+$ in the region of 65500−65650 cm^{-1} with the best simulated spectrum (second spectra from the top shown in red). The VUV-VMI-TPE spectrum for $C_3H_5^+$ was recorded at F=3.2 V/cm, achieving a FWHM of 18 cm^{-1}. The simulation is based on the selection rules that ΔK_a=odd, ΔK_c=odd for l=odd, and ΔK_a=even, ΔK_c=even for l=even, where l represents the orbital angular momentum quantum number of the outgoing photoelectron. The best simulated spectrum was obtained b assumes a Gaussian instrumental profile (FWHM=1.0 cm^{-1}), a rotational temperature of 20 K, and rotational branch ratios of N:O:P:Q:R:S:T=3:4:7:6:7:4:3.

C^+)/(A^+-C^+) for the cation, yield the value of −0.998 (−0.998) and −0.926 (−0.905) for of C_3H_3 ($C_3H_3^+$) and C_3H_5 ($C_3H_5^+$). Since the asymmetric parameters are very close to −1, both C_3H_3 ($C_3H_3^+$) and C_3H_5 ($C_3H_5^+$) can be considered as prolate symmetric top molecules. The rotational energy levels ($E_{\rm rot}$) of C_3H_3 ($C_3H_3^+$) and C_3H_5 ($C_3H_5^+$) are calculated by diagonzalizing the Hamiltonian matrix using the symmetric top rotational basis set. The intensity $I_{\rm PE}$ (J'', K_a'', K_c'') for a rotational transition from a neutral state to a cationic level is proportional to the rotational population of the neutral molecule according to the Boltzmann distribution,

$$I_{\rm PE}(J'', K_a'', K_c'') \propto r_{\rm B}(2J''+1)\exp\left(\frac{-\Delta E_{\rm rot}}{kT_{\rm rot}}\right) \quad (1)$$

where $T_{\rm rot}$ represents the rotational temperature for the molecular sample, $\Delta E_{\rm rot}$ is the rotational energy measured with respect to the ground rovibronic state of the neutral molecule, and $r_{\rm B}$ is a scaling parameter for a given rotational branch. In the electric dipole approximation for the selection rule, the conservation of the total angular momentum ignoring the electron spin gives: $|\Delta J|=|J^+-J''\leq$l+1, where l represents the orbital angular momentum quantum number of the outgoing photoelectron. The simulation takes into consideration of the rotational branches, N, O, P, Q, R, S, and T for ΔJ=0, ±1, ±2, and ±3.

The general symmetry selection rules for $C_3H_3(\tilde{X}^2B_1)$ has been discussed in detail previously [16, 17]. The symmetry analysis of the rovibronic wavefunctions for the neutral and cation shows that the rotational selection rules for the photoionization $C_3H_3^+(\tilde{X}^1A_1)\leftarrow C_3H_3(\tilde{X}^2B_1)$ are:

$$\Delta K_a = \text{odd},\ \Delta K_c = \text{even}\ \text{ for }\ l = \text{even}$$
$$\Delta K_a = \text{odd},\ \Delta K_c = \text{odd}\ \text{ for }\ l = \text{odd}$$

Figure 10 reveals the best overall simulated spectrum (second spectrum from the top) in comparison with the experimental VMI-TPE spectrum (top spectrum) obtained at F=3.2 V/cm. Since two H atoms are located symmetrically about the main molecular axis of C_3H_3, it is necessary for the neutral rotational population to take into account the nuclear spin statistics, yielding a ratio of 3:1 for even K_a'':odd K_a''. The best simulated spectrum for the formation of $C_3H_3^+$ is the sum of the rotational contributions of the Q; P and R; O and S; and N and T branches shown below the best overall simulated spectrum in Fig.10. The corresponding rotational branching ratios that give the best simulation are N:O:P:Q:R:S:T=2:3:5:3:5:3:2. The simulation also provide a rotational temperature of $T_{\rm rot}$=35 K for the C_3H_3 radical sample. The experimental VUV-VMI-TPE spectrum was simulated by assuming a Gaussian instrumental energy function (FWHM=3.5 cm^{-1}). The experimental spectrum reveals a main peak with the distinctive left and right shoulders. The main peak of the $C_3H_3^+$ origin band is contributed by the photoionization transition K_a''=0→K_a^+=1, which lies 9 cm^{-1} higher than the IE(C_3H_3) defined the photoionization transition $0_{00}\rightarrow 0^+_{0^+0^+}$. The simulation yields the IE(C_3H_3) value of 70169 cm^{-1}. Since F=3.2 V/cm

DOI:10.1063/1674-0068/29/cjcp1512247

is applied in the PI/PEX region during the TPE detection, the Stark shift correction is determined to be 5.4 cm^{-1}. Thus, the IE(C_3H_3) is determined to be 70174.4±3.5 cm^{-1}, which is in excellent agreement with the published IE values of 70175±2 and 70174.5±2.0 cm^{-1} determined by Hong *et al.* [16] and Jacovella *et al.* [17] respectively.

The general symmetry selection rules for the photoionization transition $C_3H_5^+(\tilde{X}^1A_1)\leftarrow C_3H_5(\tilde{X}^2A_2)$ have also been discussed in detail previously [35, 36]. Depending on whether the photoionization occurs out of the molecular orbital p_π or d_σ of C_3H_5 ($\tilde{X}^2A_2$), the ΔK_a and ΔK_c selection rules are

$$\Delta K_a = \text{even},\ \ \Delta K_c = \text{even}\ \text{ for }\ l = \text{even}$$
$$\Delta K_a = \text{odd},\ \ \Delta K_c = \text{odd}\ \text{ for }\ l = \text{odd}$$

Figure 11 depicts the best overall simulated spectrum (second spectra from the top) for the comparison with the experimental VMI-TPE spectrum (top spectrum) obtained at F=3.2 V/cm. The best simulated spectrum represents the sum of the contributions of the N, O, P, Q, R, S, and T-branches with the branching ratios of N:O:P:Q:R:S:T=3:4:7:6:7:4:3. The simulation yielded an estimate of 20 K for the rotational temperature $T_{\rm rot}$ of C_3H_5 radicals. The experimental VUV-VMI-TPE spectrum was simulated by a Gaussian instrumental energy function (FWHM=1 cm^{-1}). The experimental VUV-VMI-TPE spectrum for the origin band of $C_3H_5^+(\tilde{X}^1A_1)$ reveals a discernible double peak structure, which is also observed in the previous PFI-PE measurements [35, 36]. The double peak structure (separation≈5 cm^{-1}) observed in the VUV-VMI-TPE curve is less pronounced compared to that found in the previous VUV-PFI-PE, and is mainly contributed by the P and R rotational branches. The simulation yields an ionization threshold of 65580 cm^{-1} for C_3H_5. After taking into account the Stark shift of 5.4 cm^{-1} due to the applied of F field of 3.2 V/cm at the PI/PEX region, the IE(C_3H_3) is determined to be 65585±2 cm^{-1}. This latter value is also in good accord with the previous PFI-PE measurements of 65584.6±2 cm^{-1} determined by Xing *et al.* [36] and 65580.1±2.0 cm^{-1} obtained by Gasser *et al.* [35].

E. VUV-VMI-PE spectra for $C_3H_5^+$

The VUV-VMI-PE and VUV-VMI-TPE detection schemes are complimentary methods, which provide high detection sensitivity as well as high energy resolution. Although the VUV-VMI-TPE method can achieve higher energy resolution, it requires the continuous scanning over a wide VUV energy range. The VUV-VMI-PE technique has the capability of detecting photoelectrons over a broad energy range with good energy resolutions, and can avoid the time consuming and challenging task of tuning the VUV laser over a wide energy range.

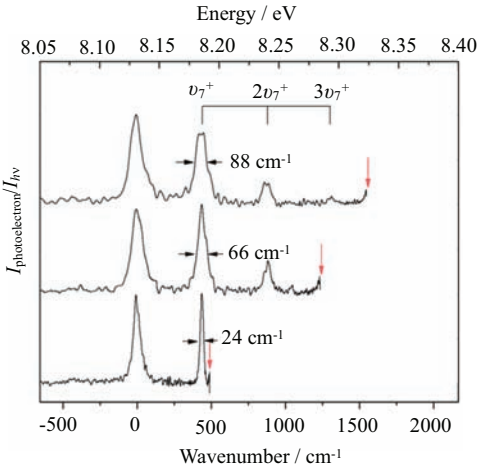

FIG. 12 The VMI-PE spectrum for $C_3H_5^+$ converted from VUV-VMI-PE images recorded at the respective VUV energies of 8.192, 8.284, and 8.323 eV (marked by downward pointing arrows). The vibrational assignments are marked by drop lines. The top scale is VUV energy in eV and the bottom energy scale is measured with respect to the origin band of $C_3H_5^+$.

The application of the VUV-VMI-PE method on radical species has been demonstrated in the previous study of $C_3H_3^+$; and the VUV-VMI-PE study of $C_3H_5^+$ has not been made. Figure 12 depicts the VUV-VMI-PE spectra for $C_3H_5^+(\tilde{X}^1A_1)$ recorded at F=33.5 V/cm and $h\nu$(VUV)=8.192, 8.284, and 8.323 eV. The photoelectron kinetic energiesof the VMI-PE spectrum were calibrated by setting the peak position of the VMI-PE origin band of $C_3H_5^+(\tilde{X}^1A_1)$ to equal the IE(C_3H_5) value of 65585±2 cm^{-1}. The VUV-VMI-PE spectra reveal discernible excitation of the υ_7^+(C−C−C bending) vibrational progression at 436,741, 876, and 1309 cm^{-1} above the $C_3H_5^+(\tilde{X}^1A_1)$ origin band [35, 36]. Similar to the comparisonof the VUV-VMI-PE spectra for $C_6H_5Cl^+$ shown in Fig.2, the VUV-VMI-PE spectra for $C_3H_5^+(\tilde{X}^1A_1)$ of Fig.12 show that the VMI-PE resolution improves as the $h\nu$(VUV) is decreased closer to the ionization threshold of C_3H_5, resulting in narrower FWHMs of the vibrational bands for $C_3H_5^+(\tilde{X}^1A_1)$ [11]. As an example, the FWHM of the υ_7^+ vibrational band was found to decrease from 88 cm^{-1} to 66 cm^{-1} to 24 cm^{-1} as the $h\nu$(VUV) energy is decreased from 8.323 eV to 8.284 eV to 8.192 eV.

IV. CONCLUSION

We have recorded the VUV-VMI-TPE and VUV-VMI-PE spectra of $C_6H_5Cl(X^1A_1)$, $C_3H_3(X^2B_1)$, and $C_3H_5(X^2A_1)$ near their ionization thresholds, aiming to establish the experimental procedures for general high-resolution photoelectron measurements of gaseous molecules. The comparison of these measurements with the corresponding VUV-PFI-PE measurements

DOI:10.1063/1674-0068/29/cjcp1512247

shows that the energy resolutions achieved in the VUV-VMI-TPE and VUV-PFI-PE detection are comparable. Since a relatively large dc field can be used to extract all photoelectrons produced, we expect the VMI-PE method to have higher detection sensitivity than that observed in the PFI-PE method. The VUV-VMI-TPE spectra of C_6H_5Cl, C_3H_3, and C_3H_5 have also been examined as a function of the applied dc electric field F employed for photoelectron extraction. The analysis of the observed Stark shift for the VUV-VMI-TPE measurements yields a Stark shift of $-3.1\sqrt{F}$ in cm^{-1}, which is half the value predicted by classical formula $-6.1\sqrt{F}$ in cm^{-1}.

V. ACKNOWLEDGMENTS

This work was supported by the National Science Foundation under CHE-0910488 and CHE-1462172. C. Y. Ng also acknowledges the support by the Chemical Sciences, Geosciences and Biosciences Division, Office of Basic Energy Sciences, Office of Science, (US) Department of Energy (DOE) under Contract No.DE-FG02-02ER15306.

[1] T. Baer, W. B. Peatman, and E. Schlag, Chem. Phys. Lett. **4**, 243 (1969).
[2] K. Mller-Dethlefs, M. Sander, and E. W. Schlag, Chem. Phys. Lett. **112**, 291 (1984).
[3] K. Muller-Dethlefs and E. W. Schlag, Annual Rev. Phys. Chem. **42**, 109 (1991).
[4] E. W. Schlag, *ZEKE Spectroscopy*, Edition Anglaise, Cambridge: Cambridge University Press, (1998).
[5] L. Zhu and P. Johnson, J. Chem. Phys. **94**, 5769 (1991).
[6] Y. C. Chang, H. Xu, Y. Xu, Z. Lu, Y. H. Chiu, D. J. Levandier, and C. Y. Ng, J. Chem. Phys. **134**, 201105 (2011).
[7] Y. Xu, B. Xiong, Y. C. Chang, and C. Y. Ng, J. Chem. Phys. **137**, 241101 (2012).
[8] Y. Xu, B. Xiong, Y. C. Chang, and C. Y. Ng, J. Chem. Phys. **139**, 024203 (2013).
[9] C. Y. Ng, Annu. Rev. Phys. chem. **53**, 101 (2002).
[10] T. Baer and Y. Li, Int. J. Mass Spectrom. **219**, 381 (2002).
[11] C. J. Hammond and K. L. Reid, Phys. Chem. Chem. Phys. **10**, 6762 (2008).
[12] H. Gao, Z. Lu, L. Yang, J. Zhou, and C. Y. Ng, J. Chem. Phys. **137**, 161101 (2012).
[13] C. Nicole, I. Sluimer, F. Rosca-Pruna, M. Warntjes, M. Vrakking, C. Bordas, F. Texier, and F. Robicheaux, Phys. Rev. Lett. **85**, 4024 (2000).
[14] A. Osterwalder, M. J. Nee, J. Zhou, and D. M. Neumark, J. Chem. Phys. **121**, 6317 (2004).
[15] D. M. Neumark, J. Phys. Chem. A **112**, 13287 (2008).
[16] H. Gao, Y. Xu, L. Yang, C. S. Lam, H. Wang, J. Zhou, and C. Y. Ng, J. Chem. Phys. **135**, 224304 (2011).
[17] U. Jacovella, B. Gans, and F. Merkt, J. Chem. Phys. **139**, 084308 (2013).
[18] X. Ripoche, P. Asselin, F. Piuzzi, and I. Dimicoli, Chem. Phys. **175**, 379 (1993).
[19] T. G. Wright, S. I. Panov, and T. A. Miller, J. Chem. Phys. **102**, 4793 (1995).
[20] C. S. Lam, H. Wang, Y. Xu, K. C. Lau, and C. Y. Ng, J. Chem. Phys. **134**, 144304 (2011).
[21] H. Woo, K. C. Lau, J. Zhan, C. Y. Ng, C. L. Li, W. K. Li, and P. M. Johnson, J. Chem. Phys. **119**, 7789 (2003).
[22] H. Gao, Y. Song, W. M. Jackson, and C. Y. Ng, J. Chem. Phys. **138**, 191102 (2013).
[23] H. Gao, Y. Song, L. Yang, X. Shi, Q. Yin, C. Y. Ng, and W. M. Jackson, J. Chem. Phys. **135**, 221101 (2011).
[24] Z. Jingang, B. Jones, Y. Xueliang, W. Jackson, and C. Y. Ng, J. Chem. Phys. **128**, 014305 (2008).
[25] X. Yang, J. Zhou, B. Jones, C. Y. Ng, and W. M. Jackson, J. Chem. Phys. **128**, 084303 (2008).
[26] J. Zhou, K. C. Lau, E. Hassanein, H. Xu, S. X. Tian, B. Jones, and C. Y. Ng, J. Chem. Phys. **124**, 034309 (2006).
[27] Y. Hou, H. K. Woo, P. Wang, X. Xing, C. Y. Ng, and K. C. Lau, J. Chem. Phys. **129**, 114305 (2008).
[28] K. C. Lau, H. Woo, P. Wang, X. Xing, and C. Y. Ng, J. Chem. Phys. **124**, 224311 (2006).
[29] B. Reed, C. S. Lam, Y. C. Chang, X. Xing, D. S. Yang, and C. Y. Ng, Astrophys. J. **693**, 940 (2009).
[30] Z. Lu, Y. C. Chang, Q. Z. Yin, C. Y. Ng, and W. M. Jackson, Science **346**, 61 (2014).
[31] A. T. J. B. Eppink and D. H. Parker, Rev. Sci. Instrum. **68**, 3477 (1997).
[32] C. J. Dasch, Appl. Opt. **31**, 1146 (1992).
[33] S. Willitsch, J. M. Dyke, and F. Merkt, Helvetica Chim. Acta **86**, 1152 (2003).
[34] S. Pratt, J. Chem. Phys. **98**, 9241 (1993).
[35] M. Gasser, A. M. Schulenburg, P. M. Dietiker, A. Bach, F. Merkt, and P. Chen, J. Chem. Phys. **131**, 014304 (2009).
[36] X. Xing, B. Reed, K. C. Lau, C. Y. Ng, X. Zhang, and G. B. Ellison, J. Chem. Phys. **126**, 171101 (2007).
[37] R. Signorell and F. Merkt, Mol. Phys. **92**, 793 (1997).
[38] S. Willitsch, A. Haldi, and F. Merkt, Chem. Phys. Lett. **353**, 167 (2002).
[39] S. Willitsch and F. Merkt, Int. J. Mass Spectrom. **245**, 14 (2005).

DOI:10.1063/1674-0068/29/cjcp1512247